PROCEEDINGS OF SCIENCE

QCD at nonzero isospin asymmetry*

Bastian B. Brandt†, Gergely Endrődi and Sebastian Schmalzbauer
Institute for Theoretical Physics, Goethe University, Max-von-Laue-Strasse 1, 60438 Frankfurt am Main, Germany
E-mail: brandt@th.physik.uni-frankfurt.de

We study the phase diagram and the thermodynamic properties of QCD at nonzero isospin asymmetry at physical quark masses with staggered quarks. In particular, continuum results for the phase boundary between the normal and the pion condensation phases and the chiral/deconfinement transition are presented. Our findings indicate that the pion condensation phase is restricted to $T \lesssim 170$ MeV for isospin chemical potentials up to 325 MeV. We also use the data to test the range of validity of the Taylor expansion method and show first results for the equation of state.

XIII Quark Confinement and the Hadron Spectrum - Confinement2018
31 July - 6 August 2018
Maynooth University, Ireland

*The research has been funded by the DFG via the Emmy Noether Programme EN 1064/2-1 and SFB/TRR 55. B.B. has also received support from the Frankfurter Förderverein für Physikalische Grundlagenforschung.

†Speaker.

PoS(Confinement2018)260

1. Introduction

Most physical systems, such as nuclei, neutron stars, and possibly the early Universe, feature an isospin asymmetry, i.e. an asymmetry between the number of up (u) and down (d) quarks. In the grand canonical ensemble, QCD with two quark flavours at finite density is described in terms of the independent isospin, $\mu_I = (\mu_u - \mu_d)/2$, and baryon, $\mu_B = (\mu_u + \mu_d)/2$, chemical potentials. The preferred tool to study QCD from first principles is Lattice QCD. While most of the parameter space with $\mu_B \neq 0$ suffers from the complex action problem, QCD with *pure* isospin chemical potential, i.e., $\mu_I \neq 0$ but $\mu_B = 0$, has a real and positive action and is amenable to Monte-Carlo simulations. In most of the physical situations the effects due to non-zero μ_B are expected to be dominant, but there are some cases where isospin might play the major role, for instance in the early universe at large lepton asymmetry [1] and for compact stars with pion condensates [2, 3]. Furthermore, studying QCD at pure isospin chemical potential is interesting in its own right. It has a rich phase diagram, shown schematically in Fig. 1, featuring a phase with Bose-Einstein condensation (BEC) of charged pions [4, 5] and a hypothetical superconducting (BCS) phase at large μ_I on top of the standard hadronic and quark-gluon plasma phases [6].

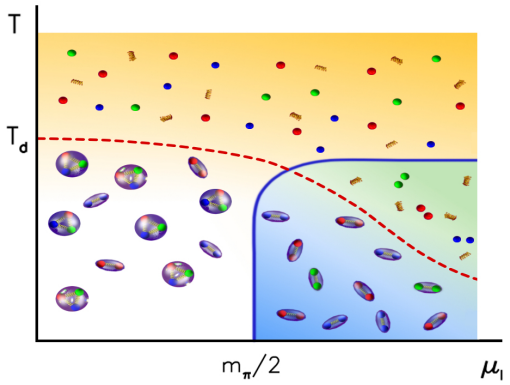

Figure 1: Conjectured phase diagram of QCD at pure isospin chemical potential (taken from [14]).

In addition, QCD at pure isospin chemical potential shares a number of technical features with QCD at finite baryon chemical potential, such as the Silverblaze phenomenon [7] and particle creation, as well as a proliferation of low modes in the BEC phase. The latter demands the introduction of an infrared regulator to facilitate simulations in the BEC phase [8, 9, 10]. A similar regulator might be necessary for simulations at non-zero μ_B beyond threshold. QCD at pure isospin chemical potential is also the ideal test system for methods such as Taylor expansion, which are commonly used to overcome the complex action problem for small μ_B.

Following the initial studies of QCD at non-zero μ_I from Refs. [8, 9, 11, 12, 13, 10], we have presented the first result for the continuum phase diagram with physical quark masses in Ref. [14] for $\mu_I \leq 120$ MeV. Essential for this study has been the introduction of a novel method for the extrapolation to vanishing regulator, λ, using the singular values of the massive Dirac operator. We also compared our results at finite value of μ_I to results obtained from Taylor expansion [15], where we also updated the results for the BEC phase boundary to $\mu_I \leq 325$ MeV. In this proceedings article we summarise the studies mentioned above and show the updated phase diagram. We also report on our ongoing measurements of the equation of state (EOS). First accounts of our results have been presented in Refs. [16, 17].

2. Simulation setup and λ-extrapolations

We study QCD at non-zero μ_I using $2+1$ dynamical quark flavours. The strange (s) quark,

has vanishing chemical potential, $\mu_s = 0$, and we employ the fourth-root trick. The fermion matrix of the light quark flavours includes a pionic source term (see [14], for instance) as a regulator, with a prefactor λ . For the simulations we use a tree-level improved Symanzik gauge action and improve the fermion action by using two steps of stout smearing. To tune the quark masses to their physical value we use the line of constant physics from Ref. [18]. In our study we use four different temporal extents, $N_t = 6$, 8, 10 and 12, corresponding to four different lattice spacings.

Our main observables to study the phase diagram are the renormalised pion and quark condensates, given by (here m_{ud} is the mass of the light quarks)

$$\Sigma_{\bar{\psi}\psi} = \frac{m_{ud}}{m_\pi^2 f_\pi^2}\left[\langle\bar{\psi}\psi\rangle_{T,\mu_I} - \langle\bar{\psi}\psi\rangle_{0,0}\right] + 1, \qquad \Sigma_\pi = \frac{m_{ud}}{m_\pi^2 f_\pi^2}\left\langle\pi^\pm\right\rangle, \tag{2.1}$$

where

$$\left\langle\pi^\pm\right\rangle = \frac{T}{V}\frac{\partial \log \mathscr{Z}}{\partial\lambda}, \qquad \langle\bar{\psi}\psi\rangle = \frac{T}{V}\frac{\partial \log \mathscr{Z}}{\partial m_{ud}}. \tag{2.2}$$

As an indicator for deconfinement we consider the renormalised Polyakov loop

$$P_r(T,\mu_I) = Z\cdot P(T,\mu_I), \quad Z = \left(\frac{P_\star}{P(T_\star,\mu_I=0)}\right)^{T_\star/T}, \quad P = \left\langle \frac{1}{V}\sum_V \mathrm{Tr}\prod_{n_t=0}^{N_t-1} U_t(n)\right\rangle \tag{2.3}$$

with $P_\star = P_r(T_\star,0) = 1$ and $T_\star = 162$ MeV. Our main observable to determine the EOS and the comparison to Taylor expansion is the isospin density

$$\langle n_I\rangle = \frac{T}{V}\frac{\partial \log \mathscr{Z}}{\partial \mu_I}, \tag{2.4}$$

which does not require renormalisation.

The simulations are done at unphysical $\lambda > 0$. Physical results are obtained in the limit of vanishing regulator $\lambda \to 0$. To this end we perform simulations at multiple values of λ and extrapolate the results to $\lambda = 0$. These extrapolations are the major challenge in the analysis, due to the pronounced λ-dependence of most of the observables. To obtain reliable λ-extrapolations over the whole parameter space and all observables mentioned above, we have introduced an improvement program for the λ-extrapolations [14]. The program is based on the singular value representation of the observables and consists of two steps: a "valence quark improvement", corresponding to a reduction of the λ-dependence of the observable, and an approximate reweighting to the $\lambda = 0$ ensemble. The remaining λ-extrapolation is mostly flat and can be carried out in a controlled manner. From now on we will always work with λ-extrapolated observables.

3. Results for the phase diagram

We start by presenting our results for the phase diagram at non-zero μ_I. The boundary of the BEC phase, $\mu_{I,c}(T)$, is determined by the points where Σ_π acquires a nonzero expectation value and the chiral crossover transition temperature $T_{pc}(\mu_I)$ by the location of the inflection point of $\Sigma_{\bar{\psi}\psi}$ with respect to T. To determine these phase boundaries, we interpolate Σ_π and $\Sigma_{\bar{\psi}\psi}$ for the individual lattices using suitable two-dimensional spline fits where the nodepoints have been generated via Monte-Carlo. For the continuum extrapolation, we parametrise the spline results

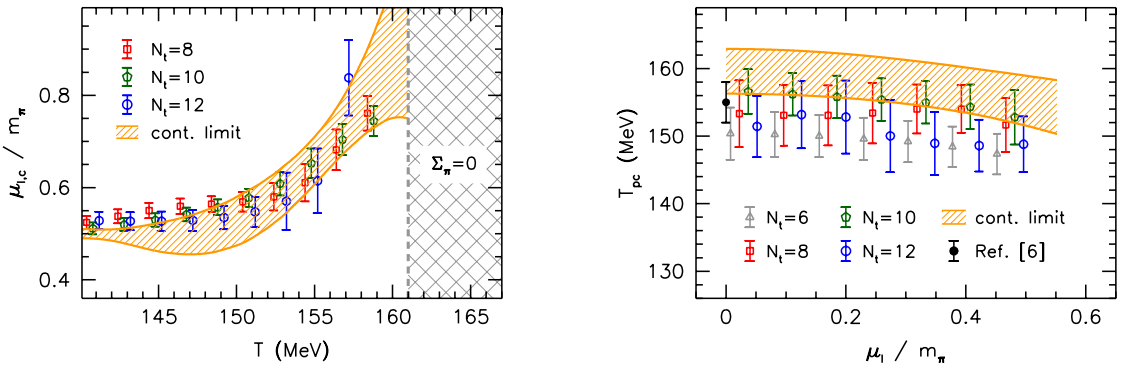

Figure 2: Continuum extrapolations for the BEC phase boundary (left panel) and the chiral crossover transition temperature (right panel). The yellow curves are the continuum extrapolations and the data points are the ones from the individual lattices which entered the fits. In the left panel, the shaded grey area represents the region where Σ_π has been found to be consistent with zero within errors for $\mu_I \leq 120$ MeV.

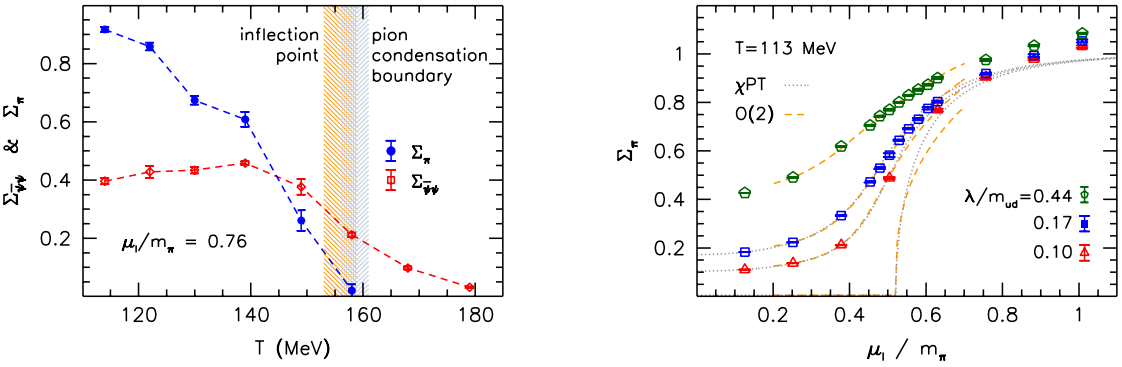

Figure 3: Left panel: Pion and quark condensates as functions of T for $\mu_I = 103$ MeV on the $N_t = 10$ ensembles. The light blue and orange areas mark the BEC phase boundary and the location of the inflection point of the condensate, respectively. Right panel: Comparison of the results for Σ_π at nonzero λ to χPT (dotted grey line) and to the critical behaviour of the O(2) universality class including scaling violations (dashed yellow line).

for $\mu_{I,c}(T)$ and $T_{pc}(\mu_I)$ by polynomials in $(T - T_0)$ (with $T_0 = 140$ MeV) and μ_I^2, respectively, including lattice spacing dependent coefficients. In both cases we found the $N_t = 6$ lattices to be outside of the scaling region. The results for the continuum extrapolations are shown in Fig. 2. For more details see Ref. [14]. The two phase boundaries meet in a pseudo-triple point at $\mu_I = \mu_{I,pt}$ and $T = T_{pt}$ and are on top of each other from that point on. This can be seen from the plot in the left panel of Fig. 3. The behaviour of Σ_π and $\Sigma_{\bar{\psi}\psi}$ with T for $\mu_I > \mu_{I,pt}$ indicates that pion condensation and chiral symmetry restoration occur at a similar temperature. A scaling analysis of Σ_π, see the right panel of Fig. 3, indicates that the transition to the BEC phase is of 2nd order in the O(2) universality class, as expected from the symmetry breaking pattern.

Recently we have also determined the BEC phase boundary for $\mu_I > 120$ MeV [15], in this region conveniently represented by a critical temperature $T_c(\mu_I)$. The continuum limit has been

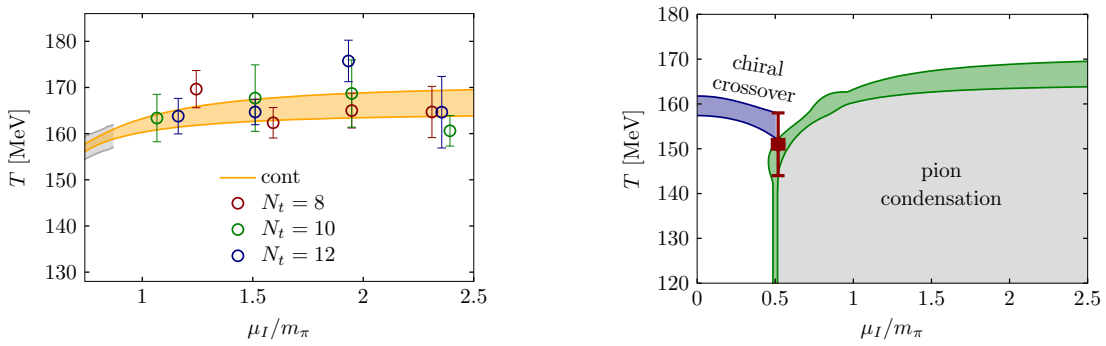

Figure 4: Left panel: Continuum extrapolation of the BEC phase boundary for $\mu_I > 120$ MeV. The yellow curve is the continuum extrapolation, the data points are from the individual lattices and the grey band is the part of the continuum extrapolation for the BEC phase boundary for $\mu_I < 120$ MeV, entering the fit for matching purpose. Right panel: QCD phase diagram for nonzero isospin chemical potential in the continuum limit. Shown are the chiral crossover transition temperature $T_{pc}(\mu_I)$ (blue band) and the boundary $\mu_{I,c}(T)$ (green band) to the BEC phase (shaded grey area). The red point is the pseudo triple point, beyond which the two transitions coincide.

performed by a fit to the form $d_1 + d_2/\mu_I^2$ with a^2-dependent coefficients d_1 and d_2. In the fit we included data from the continuum extrapolation for $\mu_I \leq 120$ MeV from Fig. 2 for $T < 161$ MeV and 90 MeV $\leq \mu_I \leq 120$ MeV, to smoothly connect the two regions of the boundary. The resulting extrapolation is shown in the left panel of Fig. 4. The updated continuum phase diagram for $\mu_I \leq$ 325 MeV is shown in the right panel of Fig. 4.

Eventually, we are also interested in a possible crossover to the BCS phase, which we expect to be related to the deconfinement transition in the BEC phase, as indicated in Fig. 1. First results on $N_t = 6$ lattices have been reported in Ref. [14]. A detailed study of the BCS phase and the deconfinement transition, however, demands large values of μ_I at smaller temperatures, which we plan to study in the near future.

4. A test for Taylor expansion

One of the possible methods to overcome the complex action problem is the aforementioned Taylor expansion method. The key idea is to expand observables around $\mu_B = 0$, so that the resulting expressions include derivatives at $\mu_B = 0$ which can be computed in direct simulations. In practice, only a finite number of expansion coefficients can be computed, so that the series has to be truncated at that order. The main problem of the method is, that the reliability region of the truncated series is unknown *a priori*. A similar expansion can also be performed in μ_I. For the isospin density, on which we will focus from now on, the expansion takes the form

$$\frac{\langle n_I \rangle}{T^3} = c_2 \left(\frac{\mu_I}{T}\right) + \frac{c_4}{6}\left(\frac{\mu_I}{T}\right)^3 + \ldots , \tag{4.1}$$

where c_2 and c_4 are the Taylor coefficients of the expansion of the pressure in μ_I/T (see Ref. [15] for the details). The Taylor coefficients for our action are available to us from Ref. [19].

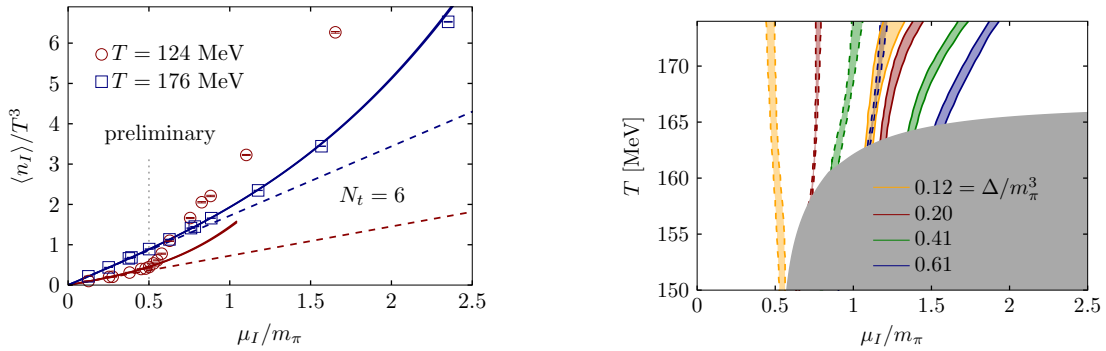

Figure 5: Left panel: Results for $\langle n_I \rangle$ at temperatures of 124 and 176 MeV on $N_t = 6$ lattices from direct simulations (red and blue points) in comparison to LO (dashed lines) and NLO (solid lines) Taylor expansions. Right panel: Contours of constant difference Δ^{LO} (dashed bands) and Δ^{NLO} (solid bands) for $N_t = 8$. The shaded grey area represents the BEC phase.

In the left panel of Fig. 5 we show the comparison between the full results for $\langle n_I \rangle$ and the Taylor expansions to leading (LO) and next-to-leading (NLO) order on the $N_t = 6$ lattices (all our data is reasonably far away from saturation with $\mu_I a < 0.3$). For $T = 124$ MeV, the data reaches the BEC phase boundary at $\mu_{I,c} \approx m_\pi/2$ and is in remarkable agreement with Taylor expansion to LO and NLO up to this point. As expected, the Taylor expansion breaks down at the boundary, showing large deviations to the lattice data. For $T = 176$ MeV the data lies above the BEC phase boundary and the agreement with Taylor expansion persists up to larger values of μ_I. At around $\mu_I/m_\pi \approx 0.6$ the data starts to favour the expansion to NLO over the LO expansion. Higher orders become important at around $\mu_I/m_\pi \approx 1.6$.

For a quantitative comparison we consider contours with a constant difference

$$\Delta^{\mathrm{LO/NLO}} = \left| \langle n_I \rangle - \langle n_I \rangle^{\mathrm{LO/NLO}} \right| \tag{4.2}$$

and focus on the high temperature region where the BEC phase transition is absent. The contour lines are, once more, determined using two-dimensional spline fits with Monte-Carlo generated nodepoints for $\Delta^{\mathrm{LO/NLO}}$. The contour lines for different values of Δ at $N_t = 8$ are shown in the right panel of Fig. 5. One can clearly see the broader range of reliability of the NLO expansion compared to the LO one and the tendency of a better performance of Taylor expansion at larger temperatures.

To investigate the range of applicability of the NLO expansion in the continuum, we extrapolate the contour lines using a second order polynomial in $(T - T_0)$ with lattice spacing dependent coefficients and $T_0 = 140$ MeV. As before, including only data with $N_t \geq 8$. The continuum contour lines are shown in the left panel of Fig. 6 versus μ_I/T. As above we observe deviations from the vertical $\mu/T = \text{const.}$ lines and the tendency for a shift to larger values of μ_I/T with increasing temperature.

The Taylor expansion can also be used to test for the existence of a phase transition at finite chemical potential, which should show up as a finite radius of convergence of the series [20]. We test this method with the BEC phase boundary. The radius of convergence r for the Taylor series

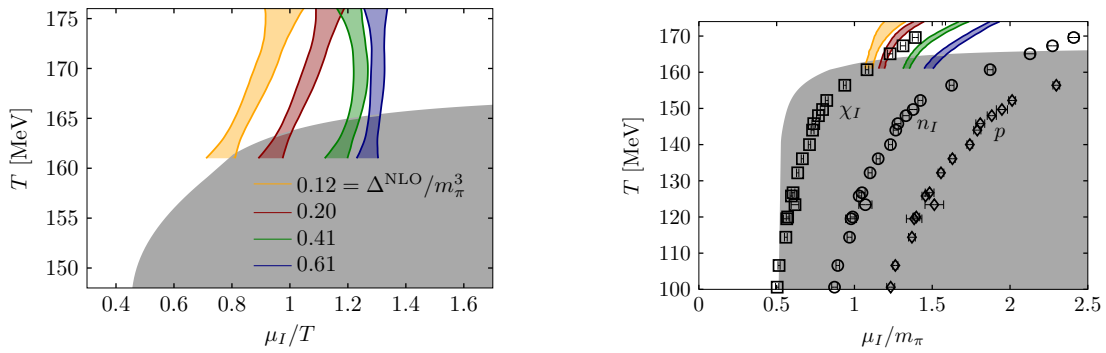

Figure 6: Left panel: Continuum results for the contours of constant difference Δ^{NLO}. The grey shaded area indicates the BEC phase. Right panel: The leading-order estimators for the radius of convergence on our $N_t = 8$ ensembles compared to the boundary of the BEC phase (grey area) and the contours of Δ^{NLO} (coloured bands).

of $\langle n_I \rangle$ can be defined as

$$r = \lim_{n\to\infty} r_n(n_I), \quad \frac{r_n(n_I)}{T} = \sqrt{\frac{c_n}{c_{n+2}}(n+1)n}\,. \tag{4.3}$$

Similar estimators for r can also be obtained from the series of the pressure p and the susceptibility $\langle \chi_I \rangle = \partial \langle n_I \rangle / \partial \mu_I$. While all estimates have to agree in the limit $n \to \infty$, they differ at finite n. Currently we have access to the $n = 2$ estimators only and, thus, cannot investigate the $n \to \infty$ limit. In Fig. 6 (right panel) we show the estimators r_2 for $N_t = 8$ from the different observables. In the vicinity of the upper BEC phase boundary, the estimators show a considerable change of slope, indicating a possible agreement of the curves in the limit $n \to \infty$[1]. It is interesting to note that $r_2(\chi_I)$ is surprisingly close to the phase boundary for low temperatures, while the other r_2 tend to overestimate r. This, likely accidental, agreement is consistent with findings in a quark-meson model [23], and in toy models of QCD with imaginary chemical potentials [24].

5. Equation of State

For the study of nuclear- and astrophysical systems, knowledge about the EOS is of fundamental importance. On top of the contribution from non-zero μ_B, it will also receive contributions from the isospin sector. Here we focus on the EOS at pure isospin chemical potential. Knowing the pressure at vanishing μ_I, all thermodynamic quantities can be determined from the n_I. In particular, the pressure can be written as

$$p(T,\mu_I) = p(T,0) + \int_0^{\mu_I} d\mu_I' n_I(T,\mu_I') \equiv p(T,0) + \Delta p(T,\mu_I)\,. \tag{5.1}$$

Knowledge about p and the trace anomaly

[1] Note, that for a general singularity in the complex μ_I-plane this limit is not guaranteed to exist – see Ref. [21] for a counter example. We also ignored subtle issues regarding the estimators of the radius of convergence at finite volumes, see Ref. [22], for instance.

$$\frac{I}{T^4} = \frac{\varepsilon - 3p}{T^4} = T\frac{\partial}{\partial T}\frac{p}{T^4} + \frac{\mu_I n_I}{T^4}, \qquad (5.2)$$

which can be extracted from p and n_I, is sufficient for the computation of all of the other thermodynamic quantities.

We evaluate $\Delta p(T, \mu_I)$ by integrating a cubic spline interpolation of the data for $\langle n_I \rangle$. The results for $\Delta p(T, \mu_I)$ at different T for $N_t = 6$ are shown in Fig. 7. Together with the results for the $\mu_I = 0$ pressure from [18] these results give the full pressure. Using this approach we calculated the EOS at $T = 0$ in [3].

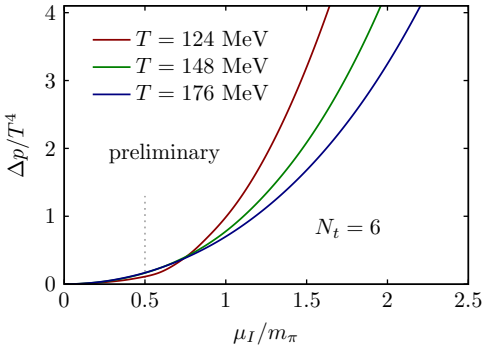

Figure 7: Results for $\Delta p(T, \mu_I)$ for different temperature values at $N_t = 6$.

References

[1] M. M. Wygas *et al*, arXiv:1807.10815 [hep-ph].

[2] A. B. Migdal, A. I. Chernoutsan and I. N. Mishustin, Phys. Lett. **83B** (1979) 158.

[3] B. B. Brandt *et al*, arXiv:1802.06685.

[4] A. B. Migdal, Rev. Mod. Phys. **50** (1978) 107.

[5] V. Ruck, M. Gyulassy and W. Greiner, Z. Phys. A **277** (1976) 391.

[6] D. T. Son and M. A. Stephanov, Phys. Rev. Lett. **86** (2001) 592 [hep-ph/0005225].

[7] T. D. .Cohen, Phys. Rev. Lett. **91** (2003) 222001 [hep-ph/0307089].

[8] J. B. Kogut and D. K. Sinclair, Phys. Rev. D **66** (2002) 014508 [hep-lat/0201017].

[9] J. B. Kogut and D. K. Sinclair, Phys. Rev. D **66** (2002) 034505 [hep-lat/0202028].

[10] G. Endrődi, Phys. Rev. D **90** (2014) no.9, 094501 [arXiv:1407.1216].

[11] J. B. Kogut and D. K. Sinclair, Phys. Rev. D **70** (2004) 094501 [hep-lat/0407027].

[12] P. de Forcrand, M. A. Stephanov and U. Wenger, PoS LATTICE **2007** (2007) 237 [arXiv:0711.0023].

[13] W. Detmold, K. Orginos and Z. Shi, Phys. Rev. D **86** (2012) 054507 [arXiv:1205.4224].

[14] B. B. Brandt *et al*, Phys. Rev. D **97** (2018) no.5, 054514 [arXiv:1712.08190].

[15] B. B. Brandt and G. Endrődi, arXiv:1810.11045.

[16] B. B. Brandt and G. Endrődi, PoS LATTICE **2016** (2016) 039 [arXiv:1611.06758].

[17] B. B. Brandt, G. Endrődi and S. Schmalzbauer, EPJ Web Conf. **175** (2018) 07020 [arXiv:1709.10487].

[18] S. Borsanyi, *et al*, JHEP **1011** (2010) 077 [arXiv:1007.2580].

[19] S. Borsanyi *et al*, JHEP **1201** (2012) 138 [arXiv:1112.4416].

[20] R. V. Gavai and S. Gupta, Phys. Rev. D **71** (2005) 114014 [hep-lat/0412035].

[21] V. Vovchenko *et al*, Phys. Rev. D **97** (2018) no.11, 114030 [arXiv:1711.01261].

[22] M. A. Stephanov, Phys. Rev. D **73** (2006) 094508 [hep-lat/0603014].

[23] F. Karsch *et al*, Phys. Lett. B **698** (2011) 256 [arXiv:1009.5211].

[24] M. D'Elia, G. Gagliardi and F. Sanfilippo, Phys. Rev. D **95** (2017) no.9, 094503 [arXiv:1611.08285].